Depósito de investigación de la Universidad de Sevilla

https://idus.us.es/

Esta es la versión aceptada del artículo publicado en:

This is an accepted manuscript of a paper published in:

Physical Review Letters (2024): 8/3/24

DOI: 10.1103/PhysRevLett.132.104004

Copyright: © 2024 American Physical Society

El acceso a la versión publicada del artículo puede requerir la suscripción de la revista.

Access to the published version may require subscription.

"This document is the Accepted Manuscript version of a Published Work that appeared in final form in [Physical Review Letters], copyright © American Physical Society after peer review and technical editing by the publisher. To access the final edited and published work see [10.1103/PhysRevLett.132.104004]."

Amplification of supersonic micro-jets by resonant inertial cavitation-bubble pair

Yuzhe Fan,[1, 2, *] Alexander Bußmann,[3, 4, *] Fabian Reuter,[1] Hengzhu Bao,[5]
Stefan Adami,[4] José M. Gordillo,[6] Nikolaus Adams,[3, 4] and Claus-Dieter Ohl[1, 2]
[1] *Faculty of Natural Sciences, Institute for Physics, Department Soft Matter,*
Otto-von-Guericke University Magdeburg,39106 Magdeburg, Germany
[2] *Research Campus STIMULATE, University of Magdeburg,*
Otto-Hahn-Straße 2, 39106 Magdeburg, Germany
[3] *Chair of Aerodynamics and Fluid Mechanics, TUM School of Engineering and Design,*
Technical University of Munich, 85748 Garching bei München, Germany
[4] *Munich Institute of Integrated Materials, Energy and Process Engineering (MEP),*
Technical University of Munich, 85748 Garching bei München, Germany
[5] *Suzhou University of Science and Technology, School of Physical Science and Technology, Suzhou 215009, China*
[6] *Área de Mecánica de Fluidos, Departamento de Ingenería Aeroespecial*
y Mecánica de Fluidos, Universidad de Sevilla, 41092 Sevilla, Spain

(Dated: May 22, 2024)

We reveal for the first time by experiments that within a narrow parameter regime, two cavitation bubbles with identical energy generated in anti-phase develop a supersonic jet. High-resolution numerical simulation shows a mechanism for jet amplification based on toroidal shock wave and bubble necking interaction. The micro-jet reaches velocities in excess of $1000\,\mathrm{m\,s^{-1}}$. We demonstrate that potential flow theory established for Worthington jets accurately predicts the evolution of the bubble gas-liquid interfaces unifying compressible and incompressible jet amplification.

Introduction: Liquid jets are encountered in various physical scenarios of collapsing cavities in liquids. Often jets are initiated by the collapse of conical or axisymmetric parabolic cavities [1, 2], e.g., by bubbles bursting near a free surface [1, 3–6], collapsing depressions of standing waves [7], the impact of water droplets on hydrophobic surfaces [8], or the impact of solids on a free surface [9–11]. In those scenarios, the cavity collapse leads to impressive amplifications of the jet velocity compared to their initiation mechanism, where the jet velocity varies from low subsonic [7–10] to supersonic states [11]. The enhancement of such energy-focusing mechanisms through the utilization of single/multiple cavities is of great importance, e.g., for alternative medical therapies of needle-based injections [12] or soft material perforation [13], where stable jets with high velocities and small volume are desired. Recently, high-speed liquid jets have been found during the evolution of single cavitation bubbles close to boundaries [14–17], where radial inward rushing liquid toward the symmetry axis induces a singularity and corresponding supersonic needle jets. However, the existence of supersonic jets during the interaction of multiple cavitation bubbles has not been reported so far.

To reveal the interaction of bubbles experimentally, we reduce the complexity to the most simple problem and study the dynamics of a single bubble pair. These have been investigated previously on different small and large scales [13, 18–20]. Han et al. [21] systematically compared experiments with simulations by varying the distance and the time interval between bubble generation. They and others have shown that the generation of similarly sized bubble pairs in anti-phase, i.e., the second bubble is generated when the first bubble is at maximum size, results in fast jets [13, 19, 21–27], where jet velocities inside the cavitation bubble of $O(100)\,\mathrm{m\,s^{-1}}$ are reached [21, 26, 27]. Focusing on the identical anti-phase bubble pair situation, in this Letter, we demonstrate experimentally and numerically that at a proper distance, the bubble pair can accelerate a needle-type jet an order of magnitude faster than formerly reported. It resembles the needle jet found in cavitation erosion studies and at elastic boundaries, yet it does not atomize but stably penetrate the gas-liquid interface.

Experimental and numerical setup: In this study, we focus on the anti-phase dynamics of bubble pairs with identical maximum radius, $R_{1,\max} = R_{2,\max} = R_{\max}$. Here, $R_{i,\max}$ are the maximum radii each bubble would reach independently, i.e., without the neighboring bubble. We control anti-phase dynamics by initiating the second bubble at $\Delta T = T_{1,\max} = T_{2,\max} = T_{\max}$, where $T_{i,\max}$ is the time when the bubble reaches its maximum size. The remaining variable parameter is the bubble seeding distance D_0, which reads in non-dimensional form $\gamma = D_0/(2R_{\max})$.

In the experiments, two bubbles are generated in deionized (DI) water through optical breakdown from two pulsed lasers (Litron Nano T-250-10; wavelength 1064 nm; pulse duration FWHM = 7 ns, and Litron Nano SG-100-2; 1064 nm; FWHM = 6 ns). The water is contained in a cuboid optical glass cuvette with squared cross section of side length of 2 cm and a height of 5 cm (Fig. 1a). Two long working distance microscope objectives facing each other focus the laser pulses. The objective lenses are mounted on three-axis micrometer stages to align the foci in the imaging plane and control

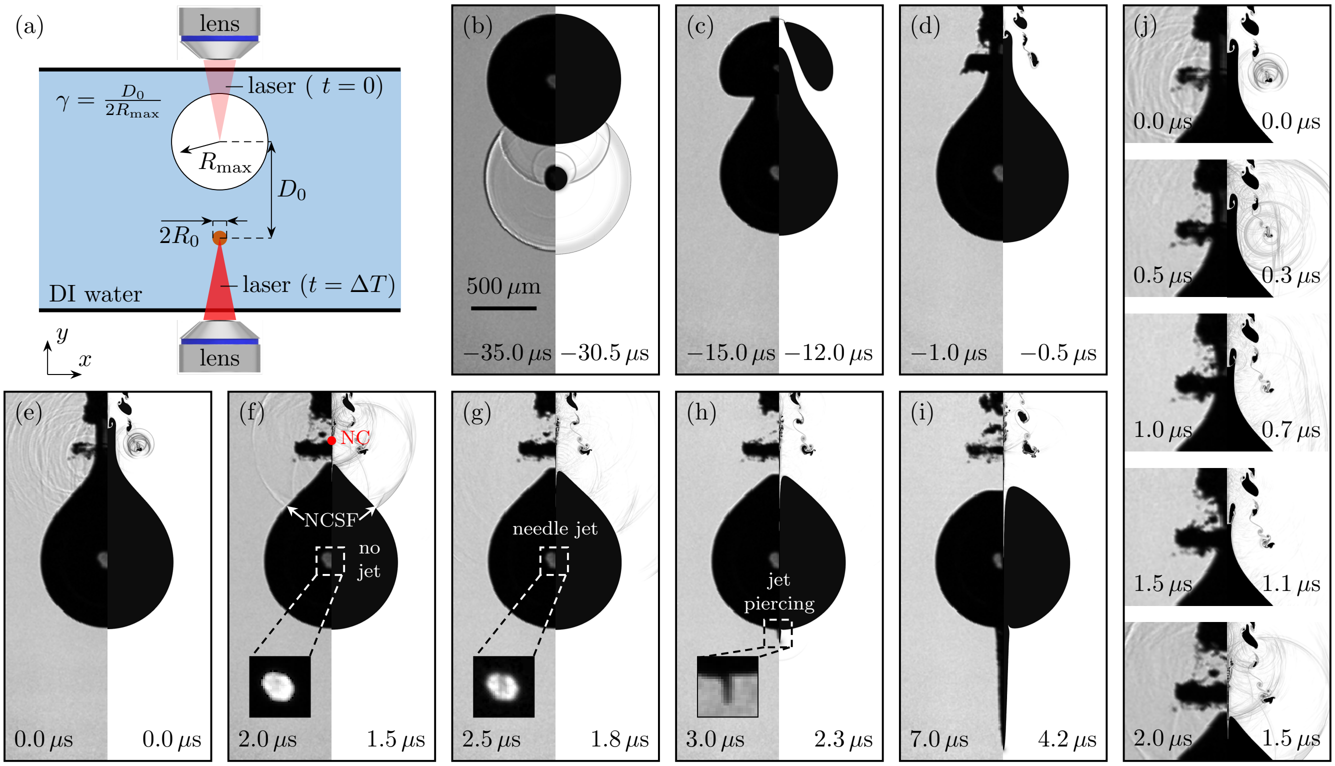

FIG. 1. **High-speed images and comparison between simulation and experiment in the ultra-fast needle jet regime for a non-dimensional standoff distance of $\gamma \approx 0.75$.** (a) Schematic representation of the camera view of the experimental set-up and the initial bubble sizes in the simulation. The upper bubble is generated first, and after $t = \Delta T \approx 46\,\mu$s, the second lower bubble is initiated. All lengths are not drawn to scale. (b-j) High-speed side-view dynamics of the experiment (left half of each image) and visualization of numerical Schlieren in the simulation (right half of each image). Note that experimental shadowgraphs show a bubble projection while the simulation shows a plane cutting the bubble, revealing more details of the bubble shape. Time instances are given in the lower corner of each image, where $t = 0\,\mu$s corresponds to the time of the torus collapse of the first bubble. In (j) a detailed view on the neck collapse between (e) and (f) is shown. In (f) the red dot marks the position of the neck collapse on the symmetry axis (NC), and the white arrows indicate the position of the neck-collapse shock front (NCSF).

the distance between the two bubbles. The dynamics of the bubbles are recorded with a high-speed camera (Shimadzu XPV-X2) at 2 million frames per second equipped with a macro lens (MP-E 65 mm f/2.8 1-5x Macro) with its magnification set to a fixed pixel resolution of 7 µm per pixel. The effective exposure time is 220 fs using an expanded pulse train from a femtosecond laser beam that illuminates the scene (Ekspla Femtolux, wavelength 515 nm).

We compare the experimental bubble dynamics with high-resolution direct numerical simulations. We employ the open-source code framework ALPACA [28–30], which solves the compressible three-dimensional Navier-Stokes equations, including viscous and capillary effects, by a Godunov-type flux-based high-order finite-volume formulation. We neglect species diffusion, gravity, and heat exchange. A conservative sharp-interface level-set method captures the interface between the cavitation bubble and the surrounding liquid. Computational costs are reduced by employing a multi-resolution scheme with timestep adaptivity and a three-dimensional axisymmetric domain. We model the bubble content by a single non-condensable ideal gas, and the surrounding water follows the Tait equation of state [16]. Bubble dynamics are represented by initial high-energetic spherical bubbles ($R_0 \approx 20\,\mu$m, $p_0 = 11\,000$ bar) that expand into water at rest (Fig. 1a). We obtain initial conditions for every initiation by matching the dynamics of a single cavitation bubble in the experiments (see supplementary material (SM)). Phase-change effects are taken into account by reducing the equilibrium radius of the first initiated bubble by 65 % at its maximum [31, 32]. This reduction rate is based on comparison of single cavitation bubble evolution in the free field between simulation and experiment (see SM). The reduction of the equilibrium radius effectively enhances the intensity of the bubble collapse. The mesh size in the simulation is sufficient to resolve the initial bubble radius with approximately $N_{\min} = R_0/\Delta x \approx 50$ cells, where Δx is the cell size. Shock wave reflections at the computational domain boundaries are suppressed by choosing the domain sufficiently large ($L = 90R_{\max}$).

Results and discussion: Figure 1b-j gives an overview of the dynamics of an anti-phase bubble pair with $\gamma \approx 0.75$, where the upper/lower bubble is initiated first/second. Composite images showing the experiment on the left and the simulation on the right half of each tile. The overall time scales of the numerical prediction were slightly different, which we associate with the simplified representation of the bubble material by a single ideal gas. Additionally, the experimental bubble appears to be slightly elongated shortly after breakdown, whereas for the simulation we initiate a spherical bubble. To compensate for the slight time-scale difference between experiment and simulation, frames of composite images are chosen in time such that both exhibit the same interface dynamics and thus correspond to the same stage of dynamics (see SM). We observe excellent agreement between simulation and experiment for the bubble dynamics and shock wave emission. Figure 1b shows images just after the initiation of the second bubble, where the plasma shock wave and its reflections are visible. While the first bubble is already shrinking, the second grows into the first, forming a long neck. This neck deforms the first bubble into a torus passing through the torus center, see Fig. 1c-e. Eventually, the first bubble collapses (Fig. 1e) and the neck of the second bubble breaks up (Fig. 1f). Immediately after neck collapse, a fast jet is ejected, as can be seen in the bubble interior, inset of Fig. 1g. Thus, it has already passed more than half of the bubble within 500 ns. It pierces the lower bubble wall (Fig. 1h), and further grows in length and radius (Fig. 1i).

Neck formation and collapse are key events in the dynamics leading to the ultra-fast needle jet. Neck formation can be seen in Fig. 1c-e. Collapse, jet formation, and piercing of the jet through the distal part of the second bubble are shown in Fig. 1g-j. The average jet velocity can be measured from the instant of formation to the instant when it is seen to have passed the bubble center. It exhibits an average velocity of $1400\,\mathrm{m\,s^{-1}}$, where from the simulations, peak velocities up to $3000\,\mathrm{m\,s^{-1}}$ can be measured immediately after jet ejection, which reduce to $1200\,\mathrm{m\,s^{-1}}$ before the jet impacts the distal side of the second bubble. After the jet has penetrated the second bubble, it remains at a reduced speed of $250\,\mathrm{m\,s^{-1}}$.

In Fig. 1j, a detailed description with finer temporal resolution of the neck breakup is shown. Shortly before the collapse of the first bubble, the neck resembles a cylindrical shape reaching its maximum elongation. Once the torus collapses ($t = 0\,\mu\mathrm{s}$), it emits a shock wave towards the elongated neck. After the shock wave emission, the neck starts to contract with a parabolic shape towards the axis of symmetry without reducing its axial neck length ($0\,\mu\mathrm{s} \leq t \leq 1.5\,\mu\mathrm{s}$). It converges radially on the symmetry axis, which results in the emission of a strong shock wave, visible in the experiment and simulation (see red dot and white arrows in Fig. 1f).

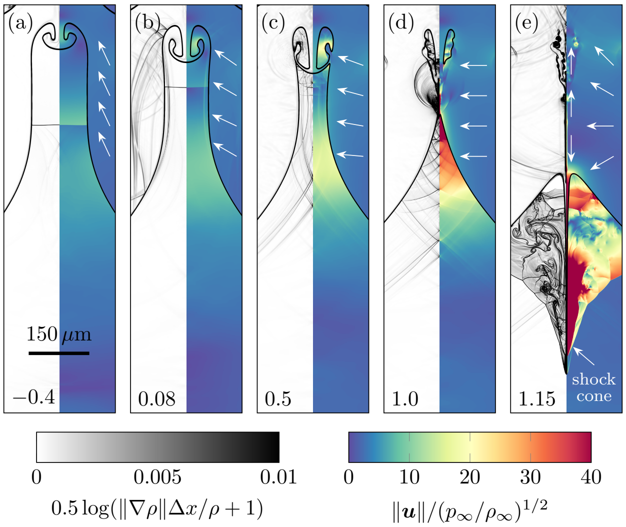

FIG. 2. **Detailed numerical representation of the ultra-fast needle jet generation dynamics shortly before and after the torus collapse.** Non-dimensional time instances are given in the lower left corner of each image, where 0 corresponds to the time of torus collapse and 1 to the time of neck breakup. The left half of each image shows non-dimensional numerical Schlieren and the right half shows the normalized velocity magnitude, where $(p_\infty/\rho_\infty)^{1/2} \approx 10\,\mathrm{m\,s^{-1}}$. The velocity field is overlaid by non-scaled white arrows indicating the flow direction. Colorbars for all images are represented at the lower part of the image.

The following illustrations give detailed insight into the neck breakup and jet formation mechanisms. We use a non-dimensional time, $t_* = (t - t_{\mathrm{tc}})/(t_{\mathrm{nc}} - t_{\mathrm{tc}})$, where t_{tc} is the time of the torus collapse of the first bubble and t_{nc} the breakup of the elongated neck. Hence, negative/positive values represent times before and after the torus collapse, respectively. The instant of neck breakup is the time when the radial flow following the collapsing neck converges on the axis of symmetry, which is detected by shock wave emission (Fig. 2d). Hence, the neck breakup is given by $t_* = 1$.

In Fig. 2, a detailed description with finer temporal resolution of the neck breakup is shown. We observe that the liquid flow velocity has a component tangential to the neck interface before the torus bubble collapses (Fig. 2a). Hence, only a small radial contraction is observed. Once the torus bubble has collapsed, the emitted toroidal shock wave impacts on the neck. This wave is partly reflected from and transmitted into the neck (Fig. 2b). The result is a contraction of the neck with a parabolic shape enhancing the radial inward motion of the surrounding liquid (Fig. 2b-d). Once the neck has contracted on the symmetry axis strong water-hammer shock waves are emitted (Fig. 2d). Finally, this high pressure region drives the flow upward/downward in the axial direction, forming the ultra-fast needle jet (Fig. 2e).

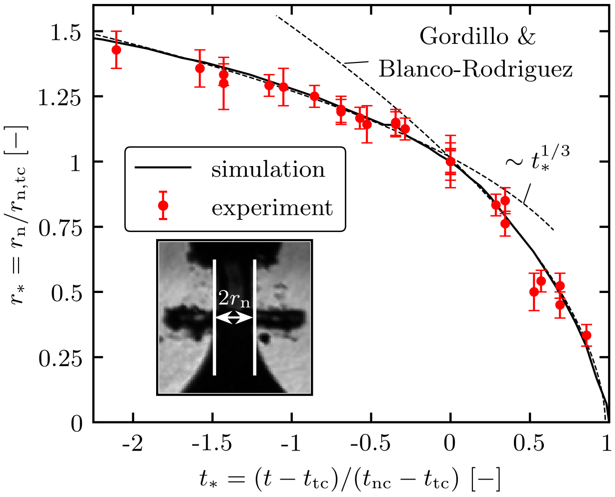

FIG. 3. **Temporal evolution of the neck radius.** Non-dimensional neck radius, $r_* = r_\mathrm{n}/r_{\mathrm{n,tc}}$, as function of the non-dimensional time, $t_* = (t - t_\mathrm{tc})/(t_\mathrm{nc} - t_\mathrm{tc})$. Here, $r_{\mathrm{n,tc}}$ is the neck radius at the time of torus collapse, t_tc, and t_nc the time of neck collapse. The measurement of the neck radius, r_n, is indicated in the image in the lower left corner. Experimental data are from different experiments within the $\gamma \in [0.72, 0.79]$ range. The line for the simulation represents a standoff distance of $\gamma \approx 0.75$. Additionally, an analytical solution of Gordillo and Blanco-Rodríguez [1] for the collapse of a parabolic cavity is shown (see SM for further details).

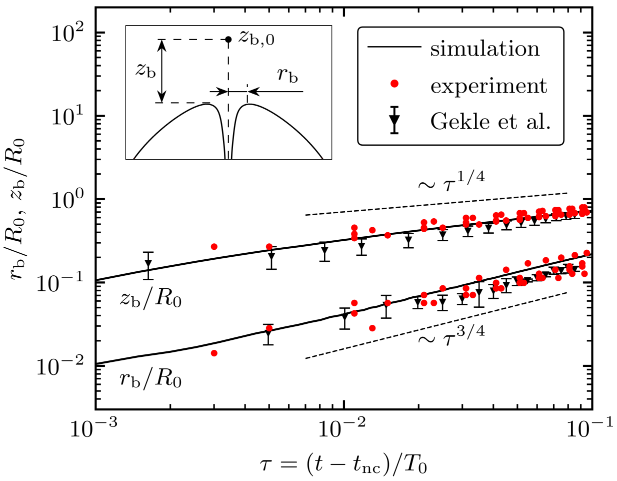

FIG. 4. **Temporal evolution of the base of the ultra-fast needle jet.** Non-dimensional jet base coordinates, r_b/R_0, and, z_b/R_0, as function of the non-dimensional time, $\tau = (t - t_\mathrm{nc})/T_0$. Here, t_nc is the time of neck collapse, $R_0 = R_\mathrm{max} \approx 500\,\mu\mathrm{m}$ the reference length, and $T_0 = R_\mathrm{max}(\rho_\infty/p_\infty)^{1/2} \approx 50\,\mu\mathrm{s}$ the reference time. A schematic sketch of the jet base geometry is given in the upper left corner, where $z_{\mathrm{b},0}$ is the axial position of the jet pinch-off. Experimental data are taken from different experiments within the $\gamma \in [0.72, 0.79]$ range, and we estimate the uncertainty for r_b/R_0 as well as z_b/R_0 as 0.02. The line for the simulation represents a standoff distance of $\gamma \approx 0.75$. Experimental data of Gekle et al. [10] are also added.

The supersonic velocity of the collapsing neck causes a conical shock wave to form inside the bubble shortly after the neck breakup (Fig. 2e). The shock cone half-angle is measured as 16 degrees, implying a jet velocity of about 3.6 times the speed of sound of the bubble content.

To further explain the mechanisms inducing the ultra-fast needle jet, Fig. 3 shows the temporal evolution of the non-dimensional neck radius, $r_\mathrm{n}/r_{\mathrm{n,tc}}$, where $r_{\mathrm{n,tc}}$ is the neck radius at torus collapse. The experimental data are given for different non-dimensional standoff distances within the $\gamma \in [0.72, 0.79]$ range. We identify two regimes: a weak contraction regime, $t_* < 0$, where the neck reduces proportional by to $t_*^{1/3}$, and a shock-accelerated regime, $t_* > 0$. Before the torus collapse, the flow field is partly tangential to the neck interface, reducing the radial contraction rate of the neck (Fig. 2a). After the impact of the torus shock wave and the impulsive acceleration of the neck, the neck radius reduces with an increased averaged slope, which agrees well with the analytical model in [33] and references therein for the collapse of a parabolic cavity.

As initial conditions, the simulated values of the neck radius, r_n, the neck velocity, $\dot{r}_\mathrm{n}$, and the radius of curvature of the neck, r_c, are taken at $t_* \approx 0.5$, where the inflow on the neck is mainly radial (Fig. 2c). The results in Fig. 3 and in the SM show that the radial flow rate per unit length, induced at the instant when the torus collapses, decreases very slowly (logarithmically), fixing the value of the flow rate per unit length, q_∞, driving the ejection of the jet [1]. Indeed, Gordillo and Blanco-Rodríguez [1] show that the time evolutions of the jet width, r_b, and the jet vertical position, z_b, after emission from an implosion of parabolic cavities are respectively given by $r_\mathrm{b} \propto \left(q_\infty^3 (t - t_\mathrm{nc})^3 / r_\mathrm{c}^2\right)^{1/4}$, and $z_\mathrm{b} \propto \left(q_\infty (t - t_\mathrm{nc}) r_\mathrm{c}^2\right)^{1/4}$. These predictions are confirmed by the experimental and numerical results depicted in Fig. 4, which exhibit the same dependence with time after a short transient. Interestingly, the results in Fig. 4 also reveal that Worthington jets produced by the incompressible collapse of parabolic cavities induced after solid impact on a free surface [10, 34] show the same time dependence as the compressible jets produced after the cavitation of bubbles. This finding can be explained by the fact that the velocity field created by an acoustic monopole at a distance $r \ll a_\infty(t - t_\mathrm{nc})$, where a_∞ represents the speed of sound in the liquid, closely resembles the one of an incompressible sink.

We observe the formation of the ultra-fast needle jet only in a narrow range of standoff distances, $\gamma \in [0.7, 0.8]$ (see SM). For larger standoff distances, $\gamma > 0.8$, the elongated neck of the second bubble does not pierce the first bubble, which prevents the impact of the torus shock wave on the neck and, consequently, a radial neck contraction. For smaller standoff distances, $\gamma < 0.7$, the neck grows in length and size, favoring unstable neck breakup with multiple breakup points on the neck surface at some radial distance to the axis of symmetry. Hence, we identify that the collapse of a parabolic cavity dominates the formation of the needle jet for equal-sized anti-phase bubble pairs. It is likely that the reported inertia-dominated mechanism of needle jet formation also applies to higher initiation energies, leading to larger bubbles and extended time-evolution periods. However, larger bubbles may be more prone to instabilities and buoyancy, affecting the flow focusing.

Summary: Based on the observations of high-speed imaging experiments and high-resolution numerical simulations, we have revealed that the dynamics of a laser-generated anti-phase bubble pair can form ultra-fast needle jets with peak velocities up to $3000\,\mathrm{m\,s^{-1}}$ reached immediately after jet ejection and reduced to $1200\,\mathrm{m\,s^{-1}}$ before the jet impacts the distal side of the second bubble. The jet remains stable after its appearance on the distal part of the second bubble. The evolution of the jet base agrees well with those observed for Worthington jets, unifying compressible and incompressible theory of jet amplification, which has been considered to be different so far. Such stable supersonic jets only emerge in a narrow range of standoff distances between the two bubbles. Only then, a singularity forms on the axis of symmetry, created by the collapse of the elongated neck of the second bubble with a parabolic shape, which is necessary for the ultra-fast needle jet formation. Shock waves emitted from the toroidal collapse of the first bubble converge towards the neck, trigger parabolic neck collapse, and further amplify jet velocity. Due to their high velocity but small size, such supersonic jets may improve technical applications, such as needle-free injections. From a more fundamental point of view, the revealed mechanism offers a path to focus kinetic liquid energy through collective and resonant inertial cavitation bubble dynamics, e.g. [35, 36].

Funding by the German Research Foundation (DFG Project No. 440395856) and the German Federal Ministry of Education and Research (Research Campus STIMULATE No. 13GW0473A). The authors gratefully acknowledge the Gauss Centre for Supercomputing e.V. for funding this project by providing computing time on the GCS Supercomputer SuperMUC-NG at Leibniz-Rechenzentrum. J.M.G. thanks project PID2020-115655GB-C21 from the Spanish MCIN/ AEI/10.13039/501100011033.

---

[*] Yuzhe Fan and Alexander Bußmann are equal contributors to this work and designated as co-first authors.

[1] J. M. Gordillo and F. J. Blanco-Rodríguez, Theory of the jets ejected after the inertial collapse of cavities with applications to bubble bursting jets, Physical Review Fluids **8**, 073606 (2023).

[2] J. Eggers, M. A. Fontelos, D. Leppinen, and J. H. Snoeijer, Theory of the collapsing axisymmetric cavity, Physical Review Letters **98**, 094502 (2007).

[3] A. M. Gañán-Calvo, Revision of bubble bursting: Universal scaling laws of top jet drop size and speed, Physical Review Letters **119**, 204502 (2017).

[4] C.-Y. Lai, J. Eggers, and L. Deike, Bubble bursting: Universal cavity and jet profiles, Physical Review Letters **121**, 144501 (2018).

[5] J. M. Gordillo and J. Rodríguez-Rodríguez, Comment on revision of bubble bursting: Universal scaling laws of top jet drop size and speed, Phys. Rev. Lett. **121**, 269401 (2018).

[6] B. Ji, Z. Yang, and J. Feng, Compound jetting from bubble bursting at an air-oil-water interface, Nature Communications **12**, 10.1038/s41467-021-26382-w (2021).

[7] B. W. Zeff, B. Kleber, J. Fineberg, and D. P. Lathrop, Singularity dynamics in curvature collapse and jet eruption on a fluid surface, Nature **403**, 401 (2000).

[8] D. Bartolo, C. Josserand, and D. Bonn, Singular jets and bubbles in drop impact, Physical review letters **96**, 124501 (2006).

[9] R. Bergmann, D. van der Meer, M. Stijnman, M. Sandtke, A. Prosperetti, and D. Lohse, Giant bubble pinch-off, Physical Review Letters **96**, 154505 (2006).

[10] S. Gekle, J. M. Gordillo, D. van der Meer, and D. Lohse, High-speed jet formation after solid object impact, Physical review letters **102**, 034502 (2009).

[11] S. Gekle, I. R. Peters, J. M. Gordillo, D. van der Meer, and D. Lohse, Supersonic air flow due to solid-liquid impact, Physical review letters **104**, 024501 (2010).

[12] J. Schoppink and D. F. Rivas, Jet injectors: Perspectives for small volume delivery with lasers, Advanced Drug Delivery Reviews **182**, 114109 (2022).

[13] V. Robles, E. Gutierrez-Herrera, L. Devia-Cruz, D. Banks, S. Camacho-Lopez, and G. Aguilar, Soft material perforation via double-bubble laser-induced cavitation microjets, Physics of Fluids **32**, 042005 (2020).

[14] C. Lechner, W. Lauterborn, M. Koch, and R. Mettin, Fast, thin jets from bubbles expanding and collapsing in extreme vicinity to a solid boundary: A numerical study, Physical Review Fluids **4**, 021601 (2019).

[15] F. Reuter and C.-D. Ohl, Supersonic needle-jet generation with single cavitation bubbles, Applied Physics Letters **118**, 134103 (2021).

[16] A. Bußmann, F. Riahi, B. Gökce, S. Adami, S. Barcikowski, and N. A. Adams, Investigation of cavitation bubble dynamics near a solid wall by high-resolution numerical simulation, Physics of Fluids **35**, 016115 (2023).

[17] A. Sieber, D. Preso, and M. Farhat, Cavitation bubble dynamics and microjet atomization near tissue-mimicking materials, Physics of Fluids **35** (2023).

[18] G. Sankin, F. Yuan, and P. Zhong, Pulsating tandem microbubble for localized and directional single-cell membrane poration, Physical review letters **105**, 078101 (2010).

[19] F. Yuan, G. Sankin, and P. Zhong, Dynamics of tandem bubble interaction in a microfluidic channel, The Journal of the Acoustical Society of America **130**, 3339 (2011).

[20] S. Zhang, S. Wang, and A. Zhang, Experimental study on the interaction between bubble and free surface using a high-voltage spark generator, Physics of Fluids **28**, 032109 (2016).

[21] B. Han, K. Köhler, K. Jungnickel, R. Mettin, W. Lauterborn, and A. Vogel, Dynamics of laser-induced bubble pairs, Journal of Fluid Mechanics **771**, 706 (2015).

[22] P. Cui, Q. Wang, S. Wang, and A. Zhang, Experimental study on interaction and coalescence of synchronized multiple bubbles, Physics of Fluids **28**, 012103 (2016).

[23] J. Luo and Z. Niu, Jet and shock wave from collapse of two cavitation bubbles, Scientific reports **9**, 1 (2019).

[24] L. W. Chew, E. Klaseboer, S.-W. Ohl, and B. C. Khoo, Interaction of two differently sized oscillating bubbles in a free field, Physical Review E **84**, 066307 (2011).

[25] W. Liang, R. Chen, J. Zheng, X. Li, and F. Lu, Interaction of two approximately equal-size bubbles produced by sparks in a free field, Physics of Fluids **33**, 067107 (2021).

[26] Y. Tomita and K. Sato, Pulsed jets driven by two interacting cavitation bubbles produced at different times, Journal of Fluid Mechanics **819**, 465 (2017).

[27] A. Mishra, C. Bourquard, A. Roy, R. Lakkaraju, P. Ghosh, and O. Supponen, Flow focusing from interacting cavitation bubbles, Physical Review Fluids **7**, 110502 (2022).

[28] N. A. Adams, S. Adami, V. Bogdanov, A. Buhendwa, A. Bußmann, N. Fleischmann, N. Hoppe, N. Hosseini, J. Kaiser, A. Lunkov, T. Paula, F. Spaeth, A. Siguenza Torres, P. Wauligmann, J. Winter, and T. Gymnich, Alpaca - adaptive level-set parallel code alpaca, `https://mediatum.ub.tum.de/1647482` (2022).

[29] N. Hoppe, S. Adami, and N. A. Adams, A parallel modular computing environment for three-dimensional multiresolution simulations of compressible flows, Computer Methods in Applied Mechanics and Engineering **391**, 114486 (2022).

[30] N. Hoppe, J. M. Winter, S. Adami, and N. A. Adams, ALPACA - a level-set based sharp-interface multiresolution solver for conservation laws, Computer Physics Communications **272**, 108246 (2022).

[31] M. Koch, C. Lechner, F. Reuter, K. Köhler, R. Mettin, and W. Lauterborn, Numerical modeling of laser generated cavitation bubbles with the finite volume and volume of fluid method, using openfoam, Computers & Fluids **126**, 71 (2016).

[32] X.-X. Liang, N. Linz, S. Freidank, G. Paltauf, and A. Vogel, Comprehensive analysis of spherical bubble oscillations and shock wave emission in laser-induced cavitation, Journal of Fluid Mechanics **940**, A5 (2022).

[33] J. M. Gordillo and F. J. Blanco-Rodríguez, Supplementary material to: Theory of the jets ejected after the inertial collapse of cavities with applications to bubble bursting jets, Physical Review Fluids **8**, 073606 (2023).

[34] S. Gekle and J. M. Gordillo, Generation and breakup of worthington jets after cavity collapse. part 1. jet formation, Journal of Fluid Mechanics **663**, 293 (2010).

[35] A. Tiwari, C. Pantano, and J. B. Freund, Growth-and-collapse dynamics of small bubble clusters near a wall, Journal of Fluid Mechanics **775**, 1–23 (2015).

[36] N. Bempedelis and Y. Ventikos, Energy focusing in shock-collapsed bubble arrays, Journal of Fluid Mechanics **900**, A44 (2020).